Applied Catalysis B: Environmental 107 (2011) 52–58

Contents lists available at ScienceDirect

Applied Catalysis B: Environmental

journal homepage: www.elsevier.com/locate/apcatb

Photocatalytic oxidation of methyl ethyl ketones over sol–gel mesoporous and meso-structured TiO_2 films obtained by EISA method

N. Arconada[a,*], Y. Castro[a], A. Durán[a], V. Héquet[b]

[a] Instituto de Cerámica y Vidrio (CSIC), Kelsen 5, Campus de Cantoblanco, 28049 Madrid, Spain
[b] Ecole des Mines de Nantes, GEPEA, UMR CNRS 6144, 4 rue Alfred Kastler, BP 20722, 44307 Nantes Cedex 3, France

ARTICLE INFO

Article history:
Received 28 March 2011
Received in revised form 15 June 2011
Accepted 24 June 2011
Available online 30 June 2011

Keywords:
TiO_2 anatase films
Sol–gel
Evaporation induced self assembly method (EISA)
Mesoporous order of the films
MEK degradation

ABSTRACT

This work reports the influence of the meso-structure of TiO_2 films in the photocatalytic oxidation of methyl ethyl ketone. Five types of TiO_2 films were prepared combining the sol–gel route with the Evaporation Induced Self-Assembly (EISA) method. Sols were prepared from titanium tetrachloride ($TiCl_4$) using different types of pore generating agents. Films characterisation was performed by Fourier Transform Infrared Spectroscopy (FTIR), Grazing X-ray diffraction (GXRD), X-ray diffraction of small angle and Transmission Electron Microscopy (FE-SEM). Environmental Ellipsometric Porosimetry (EEP) studies were performed to obtain the adsorption/desorption isotherms and calculate porous size distribution, pore volume and specific surface area (S_s) of the films. Kinetic of MEK photocatalytic oxidation data were modelled by Langmuir–Hinshelwood equation and the adsorption and kinetics constants (k and K) were calculated. Better results of MEK degradation were obtained for the Brij58 films deposited at relative humidity (RH) of 20% and 50%. The results are correlated with the porosity properties of the films.

1. Introduction

Indoor pollution is of increasing concern in urban societies since much people spend most of their time (between 70 and 90%) into closed areas (building and transports) [1–6]. Indoor air quality (IAQ) is affected by many factors among which the presence of volatile organic compounds (VOCs) are well known for their toxic effects on human health [7–9]. Currently, a great interest is focused in developing processes that can reduce or eliminate VOCs, purifying indoor environments. Photocatalytic oxidation is a promising method to destroy these compounds [10–12].

Among various semiconductors, TiO_2 is one of the best candidates for photocatalytic applications. Its band gap energy is around 3.2 eV, thus it can be photo-activated in the near UV region. It is also a relatively cheap, nontoxic and highly stable semiconductor [13,14], permitting the formation of highly reactive species that can oxidize VOCs adsorbed on the catalyst surface [10,15,16].

Numerous studies deal with TiO_2-based photocatalysts in the form of powder or pellets [17,18]. Such approach involves several technical problems like that they cannot be used in continuous engineering processes, because a step of filtration after the reaction is necessary. For this reason, TiO_2 films have been proposed. Sol–gel process is considered an efficient method to prepare uniform films [19]. This technique presents some advantages compared to other methods such as homogeneity at molecular level, easy control of the composition, low temperature of sintering, good adherence, priority crystallisation of anatase and good optical properties. Nevertheless, the reported results show that the photocatalytic efficiency of thin TiO_2 sol–gel catalysts has to be improved.

One way is to produce porous and meso-structure TiO_2 films by adding pore generating agents able to create porous structures with high specific surface area which will increase the active area, and the contact between pollutants and catalyst, thus improving the degradation of VOCs [20–28]. Evaporation Induced Self Assembly (EISA) method is reported as a suitable method to obtain mesoporous ordered films by sol–gel method [29]. This method involves the preparation of a sol containing the inorganic precursor in acidic medium and in the presence of ethanol, water and a suitable surfactant. During the deposition of the sol, the controlled evaporation of volatile solvent allows the sol to gel transition and the self-assembly of surfactant micelles, leading to a three-dimensional network deposited as a thin film with ordered mesoporous structure. The elimination of the surfactant by calcination, washing or other techniques, creates stable and ordered mesoporous films with high specify surface area [30–32].

There is some literature dealing with the photocatalytic oxidation of ketones (acetone, methyl ethyl ketone (MEK), methyl isobutyl ketone (MIBK) or methyl isopropyl ketone (MIPK)) using supported-TiO_2 catalysts, and most of these papers focuses on the

* Corresponding author. Tel.: +34 917355840; fax: +34 917355843.
E-mail address: arconada@icv.csic.es (N. Arconada).

0926-3373/$ – see front matter © 2011 Elsevier B.V. All rights reserved.
doi:10.1016/j.apcatb.2011.06.036

influence of water vapour on the degradation of these compounds [3,33]. However, the effect of the structure and characteristics of the TiO_2 catalyst have been rarely reported [34,35]. Raillard et al. has studied the influence of different types of TiO_2-based catalysts (Degussa P25 TiO_2 films on glass support, TiO_2-anatase on fibrous support, mixed SiO_2/TiO_2 deposited on cellulose supports, or dense TiO_2 sol–gel films) in the photocatalytic degradation of ketones such as MEK [24,36] and toluene [37] showing that the stabilising agent, the type of glass plates, the number of coatings and the sintering temperature are important aspects affecting the photocatalytic activity. Coronado et al. [38] studied the photocatalytic behaviour in gas phase for TiO_2 sol–gel thin films supported on glass rings using acetone and MIBK as model molecules. Finally, Vicent et al. [39] developed a special photocatalytic reactor to reduce VOCs emissions into indoor air where the catalyst comprised of Degussa P25 deposited on fibre-glass substrates. The lack of enough information in literature related to the photocatalytic properties of TiO_2 porous thin films for indoor air pollutants was an important reason to develop this work.

Thus, the aim of this work is to study the degradation of methyl ethyl ketone in gas phase using mesoporous and meso-structured TiO_2 films obtained by sol–gel method combined with the evaporation induced self-assembly method (EISA). Three types of non-ionic pore generating agents (templates) were incorporated into the sols: Pluronic (F127), polyethylene glycol hexadecyl ether P5884 (Brij58) and Triton X100 (Triton). The films were deposited by dip-coating controlling the relative humidity (RH) and the withdrawal rates. Different techniques were used to perform catalyst structural characterisation. These included Environmental Ellipsometric Porosity (EEP) measurements from which it is possible to obtain the adsorption and desorption isotherms, porosimetry and surface area analysis to determine pore size distribution, pore volume, specific surface area (S_s) and exposed surface area (S_{exp}), and TEM and Low-X-ray diffraction analysis to determine the mesoporous structure properties. A batch photocatalytic reactor was used to evaluate the photocatalytic activity of TiO_2 films in dry air at fixed temperature, and varying pollutant concentrations. The structure of the films (porosity properties and meso-porous order) and photocatalytic parameters (adsorption and kinetic constants) have been considered to correlate the film structure with the photocatalytic efficiency of the materials.

2. Experimental

2.1. Preparation of the TiO_2 sols and coatings

Titania sols were prepared using titanium tetrachloride ($TiCl_4$) as precursor, previously mixed with absolute ethanol at a molar ratio 1 $TiCl_4$:5 EtOH. Different types of surfactants as Pluronic F-127 (F127), polyethylene glycol hexadecyl ether P5884 (Brij58) and Triton X100 (Triton) dissolved in absolute ethanol were incorporated into the sol at a molar ratio of 0.005 F127:1 $TiCl_4$, 0.1 Brij58:1 $TiCl_4$ and 0.3 Triton:1 $TiCl_4$. Finally, de-ionised water was added drop by drop to the sols, up to a final oxide concentration of 27 g/L. The final molar ratios were: 1 $TiCl_4$:62.5 EtOH: (0.005, 0.1 and 0.3) Surfactant:10 H_2O.

A reference sol was also prepared following a similar process but adding only a minimum amount of surfactant to obtain a good wettability between the sol and the substrate, with a final oxide concentration of 27 g/L.

TiO_2 films were deposited onto glass-slides by dip-coating combined with the EISA method. Table 1 summarises the relative humidity and the withdrawal rate of deposition for all the compositions. In the case of F127 sols, where the relative humidity of 20–70% is indicated, the films were obtained by dipping at 20% RH,

Table 1
Composition, withdrawal rate and RH of deposition, thickness (e), refraction index (n), density, structure porosity, crystal size (D), pore volume (V_{pore}), medium pore size (Φ) and specific (S_s) and exposed (S_{exp}) surface area after the heat treatment.

Surfactant	RH (%)	Withdrawal rate (cm min^{-1})	e (nm) ±0.02	n (at λ = 700 nm) ±0.05	Structure	D (nm) ±10%	V_{pore} (%) ±5%	Φ_{medium} (nm) ±10%	S_s (m^2/cm^3) ±10%	S_s (m^2/g) (m^2) ±10%	S_{exp} (m^2) ±10%
TiO_2- Reference	20	25	150	2.06	Dense	30	–	–	–	–	–
TiO_2- Brij58	20	35	302	1.67	Meso-porous	16	40	2.8	320	125	120
TiO_2- Brij58	50	35	270	1.68	Meso-structured	19	34	1 and 2.6	315	122	110
TiO_2- F127	20–70	35	400	1.59	Meso-structured	19	45	6.4	202	87	95
TiO_2- Triton	50	11	216	1.65	Meso-porous	19	38	2.4	340	136	90

and after a first drying the RH was increased up to 70%, this being maintained for 24 h.

The glass-slides were coated with a first layer of quasi-dense SiO_2 [40,41] (thickness of ~218 nm, and refractive index of ~1.44) to inhibit the diffusion of Na^+ cations from the substrate to TiO_2 coating during heat treatment [42–44].

The films were sintered following a cycle of 130 °C/1 day and 350 °C/90 min to consolidate the structure. The dip-coating procedure was repeated and a second layer was deposited under the same conditions with a final heat treatment of 130 °C/1 day, 350 °C/3 h and 500 °C/10 min to eliminate the surfactants and to crystallise TiO_2 as anatase form.

2.2. Structural characterisation of TiO_2 coatings

The coatings were characterised by Optical Microscopy (Zeiss, HP1), Grazing incident X-ray Diffraction (range of $2\theta = 20–70°$, fixed time of 20 s/step and increment of 0.05°, Panalytical X'Pert PRO theta/theta equipment) and Fourier Transform Infrared Spectroscopy (transmission mode in frequency range of 4000–400 cm^{-1}, resolution of 2 cm^{-1}, Perkin Elmer FTIR Spectrum 100 equipment) to confirm the homogeneity, the elimination of surfactants, the crystallisation of the inorganic network as TiO_2-anatase, and to determine the crystal size using the Scherrer's equation. Finally, Transmission Electron Microscopy (Hitachi H-7100) and Low-X-ray Diffraction (range of $2\theta = 0.5–5°$, fixed time of 1.5 s/step and increment of 0.01°, Bruker D8 Advance equipment) were used to study the meso-structure of TiO_2 films.

2.3. Textural characterisation of TiO_2 coatings

Thickness (e) and refraction index (n) were measured using a Spectroscopic Ellipsometer (WVASE32 (Variable Angle Spectroscopic Ellipsometer) J.A. Co., Woollam M-2000UTM). A humidity controlled chamber was used to evaluate the variation of e and n as a function of relative humidity (from 0 to 100%). The absorption–desorption isotherms were obtained, and pore size distribution (PSD) and pore volume of the films were determined, using the Bruggeman Effective Medium Approximation (BEMA) model and the modified Kelvin's equation. Specific surface area (S_s) and exposed surface (S_{exp}) of the films were calculated following previous papers [41,45].

2.4. Photocatalytic activity of TiO_2 films

The photocatalytic activity of TiO_2 films was evaluated through the degradation of methyl ethyl ketone (MEK, Aldrich 99.5% purity) in gas phase at a fixed temperature of 30 (±1) °C. Fig. 1 shows the 12-L bath reactor used for the photocatalytic measurements. In all the experiments, four samples with a total area of 40 cm^2 were introduced into the reactor.

UV irradiation was provided by a medium pressure mercury lamp (Heraeus TQ 718 Z4, 700 W, $\lambda_{máx} = 365$ nm) refrigerated by a water cooling tube. The temperature was maintained constant using a water circulation on the outer side of the reactor. Different thermocouples were used to control the temperature at different points in the reactor. The relative humidity was fixed at 0–3%, using a dry air flow, being measured with a thermohygrometer at the beginning of each experiment. The gas was mixed in the reactor with a circulating loop fed with an all-Teflon pump (flow of 10 L/min). The pollutants were introduced in the system as liquids through a septum on the top of the reactor and were immediately volatilized. Five MEK initial concentrations between 0.06 and 1.34 g/m^3 were introduced into the reactor for each set of experiments. A gas chromatograph associated with a flame ionisation detector (GC-FID) was used to measure MEK concentrations during the experiments. Gas samples were withdrawn with airtight syringes. Blank experiments were conducted with samples and no light activation (adsorption) and with light in the absence of TiO_2 film (photolysis).

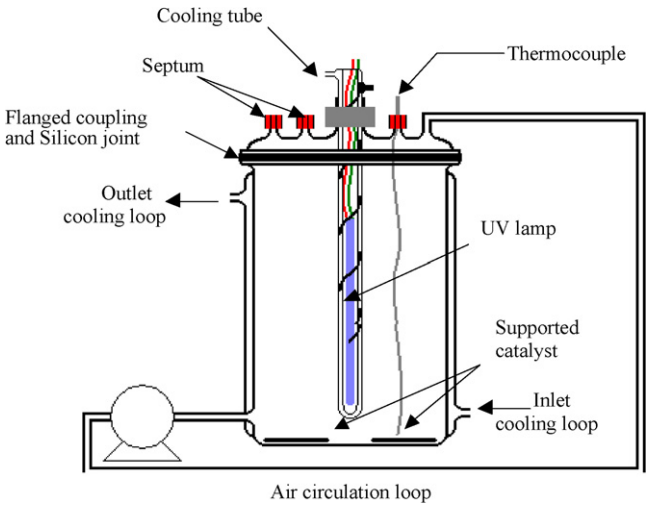

Fig. 1. Photocatalytic batch reactor.

3. Results and discussion

3.1. TiO_2 sols and catalyst characterisation

Homogeneous, transparent and stable TiO_2 sols were obtained following the process previously described [46]. TiO_2 thin films with high optical quality, transparency and without precipitates were deposited by dip-coating combined with the EISA method at different relative humidity and withdrawal rates.

The crystallisation of the inorganic network as TiO_2-anatase was confirmed by GXRD and FTIR studies. For all the coatings, the absence of TiO_2-rutile phase and the complete removal of surfactant were verified after heat treatment (Fig. 2). The crystallite size (D) of the coatings was estimated using the Scherrer's equation and the peak at $2\theta = 25.2$, selected as the main peak for determining anatase phase. Table 1 summarises the crystallite size obtained for all the films. Crystal size of 30 nm was obtained for the dense reference film and between 16 and 19 nm for the porous films, this indicating that the presence of surfactants inhibit the growth of crystallites as well as the aggregation of adjacent particles, thus resulting highly porous structures [47].

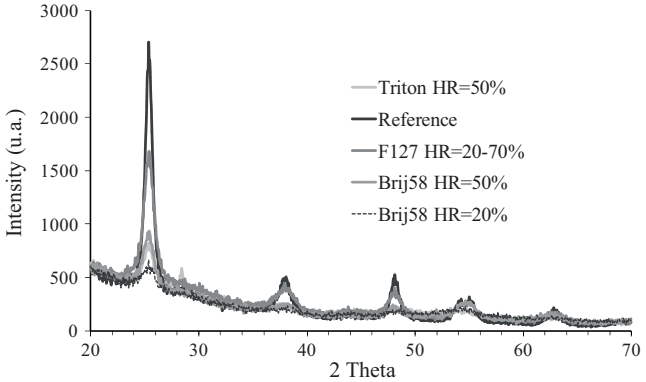

Fig. 2. GXRD spectra for the TiO_2 films obtained with the different TiO_2 sols.

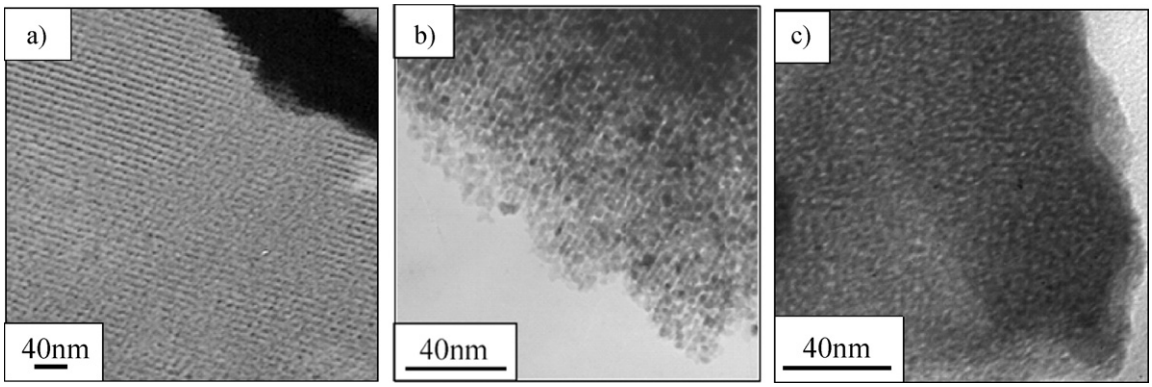

Fig. 3. TEM micrographs for the TiO_2 films obtained from sols: (a) F127 at RH 20–70%, (b) Brij58 at RH 50% and (c) Triton at RH 50%.

Transmission Electron Microscopy (TEM) and Low angle X-ray Diffraction (XRD) were used to confirm the presence of porous structures in the range of mesoporous and verify the possible order of the meso-porous films (indicated such as meso-structured film).

Fig. 3 shows the micrographs of the TiO_2 films obtained with sol (a) F127 at RH 20–70%, (b) Brij58 at RH 50% and (c) Triton at RH 50%, after the heat treatment. The films obtained with F127 sol at RH 20–70% and Brij58 sol at RH 50% show a good meso-structured porosity. However, the film obtained with Triton RH 50% shows a high porosity with homogeneous porous size, but without any order. Finally, the film obtained with the reference sol (not shown) is not porous being so considered like a reference dense film.

Low angle X-ray Diffraction patterns confirm the results obtained by TEM analysis. Fig. 4 shows the difractograms of films obtained with Brij58 sol at RH 50% and F127 sol at RH 20–70%, showing two peaks, around $2\theta = 0.8^\circ$ for Brij58 and around $2\theta = 1.8^\circ$ for F127, both associated with the ordered porosity. The presence of peaks in this range indicates the ordered mesoporosity of the films. The 2θ value of the peak was used to calculate the layer-to-layer distance, d. In the case of F127 coating deposited at RH 20–70%, $d = 5.1 \pm 0.1$ nm, whereas for Brij58 sol at RH 50% $d = 12.4 \pm 0.3$ nm.

Table 1 summarises the structural data obtained by TEM and Low-X-ray Diffraction for all the coatings indicating as dense, mesoporous or meso-structured coatings.

3.2. Textural properties of TiO_2 coatings

Spectral ellipsometry and Environmental Ellipsometric Porosimetry (EEP) measurements were used to determine thickness, refractive index and porosity properties of the films. This is a non destructive method based on the adsorption–desorption isotherms obtained from the variation of thickness and refractive index induced by the change of water partial pressure above a film [45].

Fig. 5 shows the adsorption–desorption isotherms obtained by EEP Approximation model (BEMA) along with PSD for the films obtained with the TiO_2 sols (a) Brij58 at RH 20%, (b) Brij58 at RH 50%, (c) F127 at RH 20–70% and (d) Triton at RH 50%. A typical behaviour of mesoporous materials (pore diameter range between 2 and 50 nm), associated with isotherms of type IV, is observed for all the coatings. For Fig. 4a–d the isotherms present hysteresis loops related with the capillary condensation of water that occurs in the meso-pores. According to IUPAC, hysteresis loops are classified into four types (H1–H4). Type H1 loop exhibits parallel and nearly vertical branches, characteristic of materials with cylindrical pore geometry and/or a highly uniform pore size. Hysteresis loops of type H2 present triangular shape and a steep desorption branch attributed to pore connectivity effects [48] which are often considered a result of the presence of pores with narrow mouths (bottle-neck pores) [49]. Coming back to Fig. 5, hysteresis loops H1 are identified in Fig. 5a, c and d and H2 in Fig. 5b [49,50].

Fig. 5 also includes the corresponding PSD, determined using the Kelvin's equation [45]. Total volume of pores between 30 and 45 vol.% and pore size distributions in the range 2.4–6.4 nm were obtained for all the films. Triton at RH 50% films show a broad pore size distribution and the lower hysteresis loop in the isotherms indicates smaller medium pore size (2.4 nm). On the other hand, F127 at RH 20–70% coatings present narrower pore size distribution and meso-structured porosity. Finally, meso-structured films prepared with Brij58 at RH 50% show a bimodal pore size distribution, with pores around 1 nm and 2.6 nm, the former indicating the presence of bottle-neck pores.

Specific surface area (S_s) was calculated considering an ellipsoidal-sphere geometry pore and using the slope $\beta_{mesoporous}$ of the t-plot curve, as well as the pore size (ϕ) and pore volume (V_{pore}) [45]. Finally, the exposed area (S_{exp}) has been estimated taking into account the specific surface area, S_s [m^2/cm^3] and the thickness (in cm) per 1 cm^2 of surface sample. This last parameter represents the total area exposed to irradiation, thus being relevant to photocatalytic behaviour.

Table 1 summarises the values of pore size, pore volume and specific and exposed surface areas (S_s, S_{exp}) for all the films.

3.3. MEK photocatalysis oxidation

Photocatalytic degradation kinetic studies of MEK were performed on the five photo-catalyst coatings. The photocatalytic experiments were carried out with five different MEK concentrations, at fixed temperature (30 °C), under fixed dry atmospheric conditions (RH ≤ 3%) and UV radiation. MEK initial concentrations were in the range of 0.06–1.34 g/m^3. Fig. 6 shows the decrease of MEK concentration (C (g/m^3)) with the irradiation time with the films Brij58 at RH 50%.

In photocatalytic studies, the kinetics of degradation are generally represented by the Langmuir–Hinshelwood (L–H) model, defined by the following (Eq. (1)):

$$r_0 = \frac{kKC_0}{1 + KC_0} \quad (1)$$

where r_0 is the initial reaction rate (g/(m^3 min)), k the reaction kinetic constant (g/(m^3 min)), and K is the Langmuir adsorption constant (1/(m^3 g)).

Blank experiments for the degradation of MEK ($C_0 = 0.34$ g/m^3) were performed under dry air and ambient temperature, without UV irradiation (adsorption in dark conditions) and without TiO_2 films under irradiation (photolysis) for all the tested films. The aver-

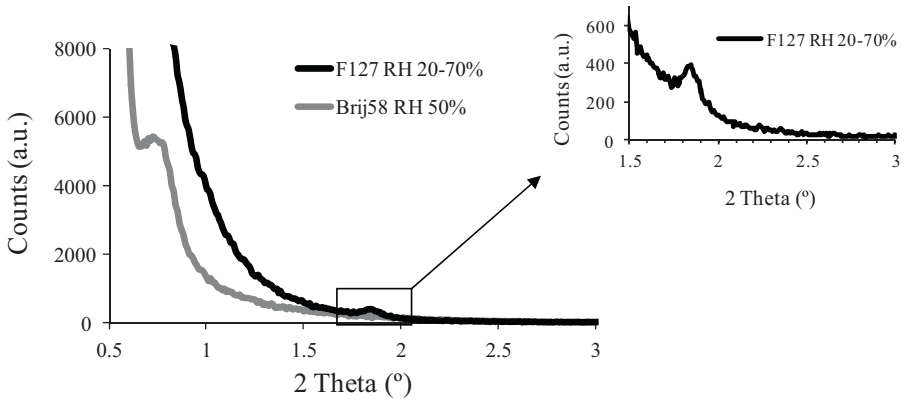

Fig. 4. XRD small angle spectra for the TiO_2 films obtained with Brij58 sol at RH 50% and F127 sol at RH 20–70%.

age values of photolysis (UV only) and adsorption (without UV) tests were around 5 and 10%, respectively.

On the other hand, for photocatalytic studies in the presence of both UV and TiO_2 films, photocatalytic degradation rates of MEK were determined for all the photocatalysts tested after periods of measurement of 150 min.

The initial reaction rates (r_0) were calculated for each experiment by modelling the kinetics of degradation by a third-order polynomial and its derivative form at initial time $r_0 = (dC/dt)_{t=0}$. The Langmuir–Hinshelwood constants were determined by least square analysis. Fig. 7 shows the experimental points modelled by the Langmuir–Hinshelwood equation for all the photocatalysts.

Table 2 summarises the percentage of adsorption, L–H model adsorption, kinetic constants and kinetic constant normalized per cm^2 of film, obtained for all the photocatalysts.

The results of the different tested materials can be explained from the kinetics and also from the absorption values. Based on the kinetic constant (k), Brij58 at RH 20% films exhibited the best photocatalytic activity, followed by Brij58 at RH 50%, associated with the highest specific and exposed surface areas. On the other hand,

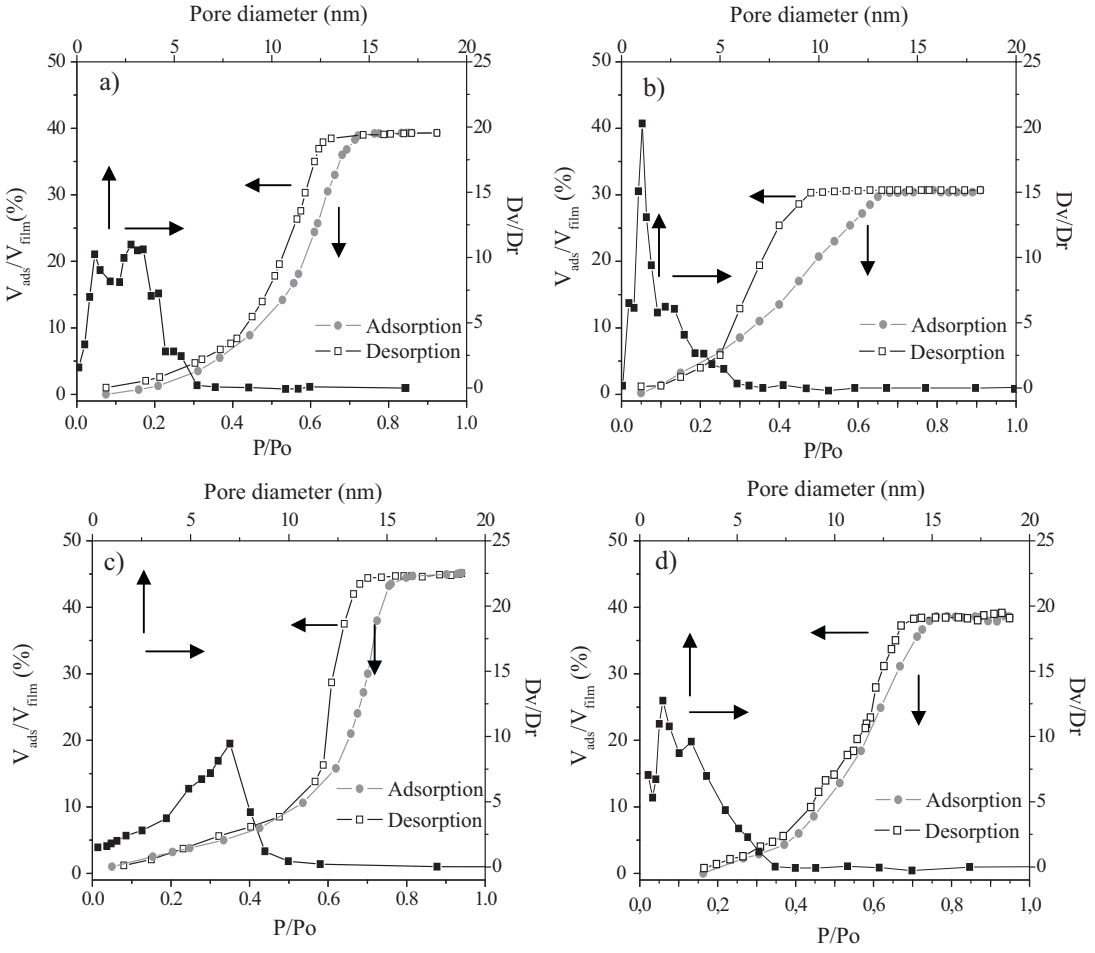

Fig. 5. Adsorption/desorption isotherms (●, □ axes: V_{ads}/V_{film} vs P/P_0) and pore size distribution (■ axes: Dv/Dr vs pore diameter) for the TiO_2 films obtained from sols; (a) Brij58 at RH 20%, (b) Brij58 at RH 50%, (c) F127 at RH 20–70% and (d) Triton at RH.

Table 2
Composition, Langmuir–Hinshelwood kinetic (k) and adsorption (K) constants, for all the photocatalysts.

Surfactant	$RH_{deposition}$ (%)	Langmuir–Hinshelwood constants determination			
		k (g/(m^3 min))	k ($\times10^{-4}$) (g/(m^3 min^{-1}))/cm^2 films	K (1/(m^3 g))	R^2
TiO_2- Reference	20	0.0027 (±0.0003)	2.2 (±0.2)	10.0 (±2.85)	0.975
TiO_2- Brij58	20	0.0044 (±0.0003)	3.5 (±0.2)	4.3 (±0.83)	0.991
TiO_2- Brij58	50	0.0028 (±0.0001)	2.2 (±0.8)	16.6 (±3.48)	0.983
TiO_2- F127	20–70	0.0024 (±0.003)	1.9 (±0.2)	3.6 (±1.55)	0.977
TiO_2- Triton	50	0.0026 (±0.0003)	2.4 (±0.2)	7.8 (±3.05)	0.978

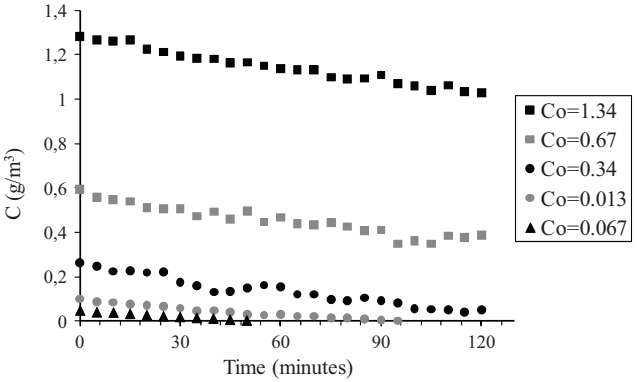

Fig. 6. MEK concentration (C (g/m^3)) vs irradiation time (min) for the TiO_2 films of Brij58 at RH 50%.

the adsorption constant (K) was the highest for Brij58 at 50% films followed by Reference > Triton at RH 50% > Brij58 at RH 20% > F127 at RH 20–70% films.

The initial reaction rate (r_0) of MEK degradation was a function of the initial concentration of MEK contaminant. At low concentration, the kinetics are controlled by mass transfer (adsorption) of the molecule and the materials with higher adsorption constant K will be the most efficient. However, at high contaminant concentrations the kinetic constant k controls the reaction rate since the surface is often near saturation; thus, materials with higher k will show the highest photocatalytic capacity.

In our samples, Brij58 at RH 20% films exhibited the highest degradation at high initial concentration while Brij58 at RH 50% samples demonstrated the most efficient behaviour at lower initial MEK concentration. The other tested films show the same order at low and high MEK concentrations. The efficiency of the photocatalysis follows the order Reference > Triton RH 50% > F127 RH 20–70%.

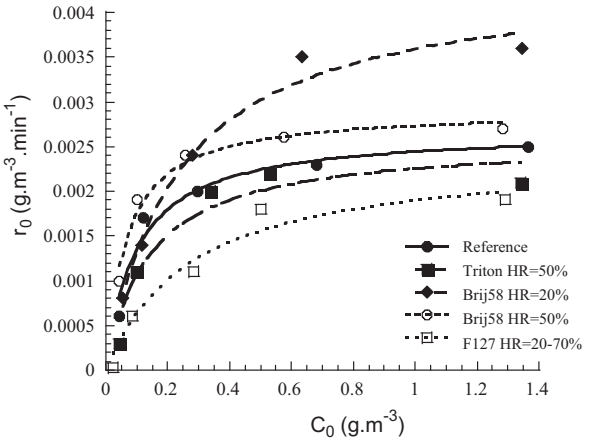

Fig. 7. r_0 vs C_0 for the photocatalysts and the reference modelled by Langmuir–Hinshelwood equation.

The different photocatalytic behaviour observed between Brij58 at RH 20% and RH 50% could be explained considering the adsorption–desorption isotherms and PSD. In the case of meso-structured Brij58 at RH 50% films, the presence of a pore size distribution of 2.6 nm pores along with bottle necks 1 nm in size may justify the high efficiency at low MEK concentrations; for increasing pollutant concentration, the narrow bottle-necks will rapidly arrive to saturation by adsorption of molecules thus causing decrease in photocatalytic activity. On the other hand, Brij58 at RH 20% films possess a similar pore size distribution without pore narrowing. Thus, the efficiency will increase at higher MEK concentrations achieving faster photocatalytic degradation.

Finally, films of Triton at RH 50% and F127 at RH 20–70% demonstrated behaviours similar to that of the dense TiO_2-anatase material. Triton films show a similar PSD and wide pore size range, although the lower hysteresis indicates smaller pore size. On the other hand, Triton films have thickness of only 216 nm and are the thinnest among all the studied coatings. This means that the exposed area, close related to thickness, is smaller, likely explaining the rapid saturation through adsorption. In the case of F127 samples, their poor photocatalytic behaviour could be related to the lower specific and exposed surface areas compared to Brij58 films, resulting from its larger pore size. Chen and Dionysiou [51] have demonstrated that photo-catalysts with pore size higher than 4 nm show lower photo-catalytic activity [52]. Moreover, the orientation of pore channels is often referred as parallel to the substrate [53,54], thus likely hindering the access of the pollutant to the porous structure. The control of the porosity orientation is thus a key feature to solve, in order to improve the photocatalytic behaviour of these materials.

4. Conclusions

- Mesoporous TiO_2-anatase films were prepared combining the sol–gel route with the EISA method using F127, Brij58 and Triton as surfactants.
- FTIR and GXRD confirmed the tetragonal TiO_2-anatase phase as only crystalline phase in all the films. F127 at RH 20–70% and Brij58 at RH 50% films exhibited a well defined meso-structure confirmed by low angle XRD and TEM.
- Spectral ellipsometry and Environmental Ellipsometric Porosimetry (EEP) were used to calculate the adsorption–desorption isotherms and to estimate total pore volumes between 30 and 45%, PSD around 2.4–6.4 nm, and exposed surface areas of 90–120 m^2.
- The photocatalytic behaviour of MEK degradation depends on the initial concentration of contaminant and the textural properties of the films such as pore volume, specific and exposed surface areas.
- Brij58 at RH 50% films exhibited the highest photocatalytic activity at lower initial MEK concentration while Brij58 at RH 20% coatings demonstrated the highest degradation at high MEK initial concentration. Results from pore distribution analysis suggest that the meso-structured films Brij58 at RH 50% possess narrow bottle-necks pores which contribute to achieve faster saturation

at increasing pollutant concentration; which justifies the high photocatalytic activity obtained with these films at low MEK concentrations.

- Fast MEK degradation was obtained for all the catalyst with only a small contribution from photolysis (around 5%), although the highest photocatalytic activity was attained for films Brij58 at RH 20% and RH 50%.
- These results demonstrate that this type of coatings constitutes promising systems to destroy MEK and other pollutants to be further evaluated for indoor air quality (IAQ) applications.

References

[1] S.K. Brown, M.R. Sim, M.J. Abramson, C.N. Gray, Indoor Air 4 (1994) 123.
[2] Y.M. Kim, S. Harrad, R.M. Harrison, Environ. Sci. Technol. 35 (2001) 997.
[3] C. Raillard, V. Héquet, P. Le Cloirec, J. Legrand, J. Photochem. Photobiol. A: Chem. 163 (2004) 425.
[4] C.H. Ao, S.C. Lee, C.L. Mak, L.Y. Chan, Appl. Catal. B: Environ. 42 (2003) 119.
[5] E. Righi, G. Aggazzotti, G. Fantuzzi, V. Ciccarese, G. Predieri, Sci. Total Environ. 286 (2002) 41.
[6] P. Pichat, J. Disdier, C. Hoang-Van, D. Mas, G. Goutailler, C. Gaysse, Catal. Today 63 (2000) 363.
[7] T. Salthammer, M. Bednaerk, F. Fuhrmann, R. Funaki, S.-I. Tanabe, J. Photochem. Photobiol. A: Chem. 152 (2002) 1.
[8] B. Son, P. Breysse, W. Yang, Environ. Int. 993 (2002) 1.
[9] S.C. Lee, W.-M. Li, C.-H. Ao, Atmos. Environ. 36 (2002) 225.
[10] J. Peral, X. Domenech, D.F. Ollis, J. Chem. Technol. Biotechnol. 70 (1997) 117.
[11] J. Peral, X. Domenech, D.F. Ollis, J. Mol. Catal. A: Chem. 15 (1997) 347.
[12] V. Héquet, C. Gonzalez, P. Le Cloirec, Water Res. 35 (2001) 4253.
[13] S. Suárez, J.M. Coronado, R. Portela, J.C. Martín, M. Yates, P. Ávila, B. Sánchez, Environ. Sci. Technol. 42 (2008) 5892.
[14] G. Balasubramanian, D.D. Dionysiou, M.T. Suidan, V. Subramanian, I. Baudin, J.M. Laıne, J. Mater. Sci. 38 (4) (2003) 823.
[15] D.F. Ollis, E. Pelizzetti, N. Serpone, Environ. Sci. Technol. 25 (1991) 1522.
[16] W.A. Jacoby, D.M. Blake, J.A. Fennell, J.E. Boulter, L.M. Vargo, M.C. George, S.K. Dolberg, J. Air Waste Manage. Assoc. 46 (1996) 891.
[17] J. Zhao, X. Yang, Build. Environ. 38 (2003) 645.
[18] M. Anpo, Res. Chem. Intermed. 11 (1989) 67.
[19] R.-D. Sun, A. Nakajima, T. Watanabe, K. Hashimoto, J. Photochem. Photobiol. A 154 (2003) 203.
[20] K. Yoo, H. Choi, D.D. Dionysiou, Chem. Commun. 17 (2004) 2000.
[21] H. Choi, E. Stathatos, D.D. Dionysiou, Thin Solid Films 510 (2006) 107.
[22] H. Choi, E. Stathatos, D.D. Dionysiou, Appl. Catal. B: Environ. 63 (2006) 60.
[23] Y. Chen, E. Stathatos, D.D. Dionysiou, Surf. Coat. Technol. 202 (2008) 1944.
[24] H. Choi, E. Stathatos, D.D. Dionysiou, Desalination 202 (2007) 199.
[25] N. Quici, M.L. Vera, H. Choi, G. Li Puma, D.D. Dionysiou, M.I. Litter, H. Destaillats, Appl. Catal. B: Environ. 95 (2010) 312.
[26] V. Puddu, H. Choi, D.D. Dionysiou, G. Li Puma, Appl. Catal. B: Environ. 94 (2010) 211.
[27] Y. Chen, S. Lunsford, D.D. Dionysiou, Thin Solid Films 516 (2008) 7930.
[28] M.G. Antoniou, P.A. Nicolaou, J.A. Shoemaker, A.A. de la Cruz, D.D. Dionysiou, Appl. Catal. B: Environ. 91 (2009) 165.
[29] J. Brinker, Y.L.A. Sellinger, H. Fan, Adv. Mater. 11 (1999) 579.
[30] L. Nicole, C. Boissiere, D. Grosso, A. Quach, C. Sanchez, J. Mater. Chem. 15 (2005) 3598.
[31] Aksay, M. Trau, S. Manne, I. Honma, N. Yao, L. Zhou, P. Fenter, P. Eisenberger, S. Gruner, Science 273 (1996) 892.
[32] H. Yang, N. Coombs, I. Sokolov, G.A. Ozin, Nature 381 (1996) 589.
[33] C. Raillard, V. Héquet, P. Le Cloirec, J. Legrand, Appl. Catal. B: Environ. 59 (2005) 213.
[34] C. Raillard, V. Héquet, P. Le Cloirec, J. Legrand, Water Sci. Technol. 53 (11) (2006) 107.
[35] P. Monneyron, M.-H.J. Manero, N. Foussard, F.M. Benoit-Marquié, T. Maurette, Chem. Eng. Sci. 58 (2003) 971.
[36] C. Raillard, V. Héquet, P. Le Cloirec, J. Legrand, Water Sci. Technol. 50 (4) (2004) 241.
[37] C. Stavrakakis, C. Raillard, V. Héquet, P. Le Cloire, J. Adv. Oxid. Technol. 10 (1) (2007) 94.
[38] J.M. Coronado, M.E. Zorn, I. Tejedor-Tejedor, M.A. Anderson, Appl. Catal. B: Environ. 43 (2003) 329.
[39] G. Vicent, A. Queffeulou, P.M. MArquaire, O. Zahraa, J. Photochem. Photobiol. A: Chem. 191 (2007) 42.
[40] M. Guglielmi, S. Zenezini, J. Non-Cryst. Solids 121 (1990) 303.
[41] N. Arconada, Y. Castro, A. Durán, Appl. Catal. A: Gen. 385 (2010) 101.
[42] H.-J. Nam, T. Amemiya, M. Murabayashi, K. Itoh, J. Phys. Chem. B 108 (2004) 8254.
[43] M. Nocuń, D.S. Burcon, Siwulski Opt. Appl. XXXVIII (1) (2008) 172.
[44] P. Novotna, J. Krysa, J. Maixner, P. Kluson, P. Novak, Surf. Coat. Technol. 204 (2010) 2570.
[45] C. Boissiere, D. Grosso, S. Lepoutre, L. Nicole, A.B. Bruneau, C. Sanchez, Langmuir 21 (2005) 12362.
[46] N. Arconada, Y. Castro, A. Durán, Bol. Soc. Esp. Ceram. Vidrio 49 (6) (2010) 405.
[47] I. Hyeok Choi, Thesis, Sunghyunkwan University in Korea, 2007.
[48] H. Liu, L. Zhang, N.A. Seaton, J. Colloid Interface Sci. 156 (1993) 156.
[49] Q. Huo, D.I. Margolese, G.D. Stucky, Chem. Mater. 8 (1996) 1147.
[50] M. Kruk, M. Jaroniec, A. Sayari, Langmuir 13 (1997) 6267.
[51] Y. Chen, D.D. Dionysiou, Appl. Catal. B: Environ. 69 (2006) 24.
[52] D.S. Kim, S.J. Han, S.-Y. Kwak, J. Colloid Interface Sci. 316 (2007) 85.
[53] P. Yang, D. Zhao, D.I. Margolese, B.F. Chmelka, G.D. Stucky, Chem. Mater. 11 (1999) 2813.
[54] S.W. Boettcher, M.H. Bartl, J.G. Hu, G.D. Stucky, J. Am. Chem. Soc. 127 (2005) 9721.